The 2010 M_W 8.8 Maule Megathrust Earthquake of Central Chile, Monitored by GPS

C. Vigny, *et al.*

Science **332**, 1417 (2011);
DOI: 10.1126/science.1204132

induced vertical oscillations throughout the 0.1- to 3-bar range and enhanced condensation at the cool peaks of the wave, extending east from the central vortex.

Thermal imaging of this intense northern springtime disturbance revealed strong coupling between the tropospheric outburst [possibly moist convection initiated within water clouds at 9 to 12 bar (*18*)] and the atmospheric structure between 1 mbar and 3 bar (vertically separated by 350 km) over an enormous area of Saturn's northern mid-latitudes. The increased insolation after the spring equinox (August 2009, $L_s = 0°$) may permit convective outbursts to penetrate to higher altitudes than during other seasons, where they become accessible to infrared remote sensing; but the initial instability presumably occurred at deep levels where solar insolation has no influence. The large amplitude of the stratospheric perturbations, which continue to dominate Saturn's infrared emission at the time of writing, suggests a strong atmospheric response to the storm cells below and implies vertical coupling over hundreds of kilometers between the convective deep atmosphere and the radiatively cooled upper atmosphere. Such large perturbations substantially altered atmospheric circulation, transporting energy and material vertically over great distances, perturbing stratospheric zonal jets, exciting wave activity, and disrupting the slow seasonal evolution of Saturn's atmosphere. The newly formed oval and the aftermath of this planetary disturbance could affect Saturn's northern hemisphere for years to come.

References and Notes

1. A. R. Vasavada, A. P. Showman, *Rep. Prog. Phys.* **68**, 1935 (2005).
2. A. D. Del Genio *et al.*, in *Saturn from Cassini-Huygens* (Springer Verlag, Dordrecht, Netherlands, 2009), chap. 6.
3. A. R. Vasavada *et al.*, *J. Geophys. Res. Planets* **111**, E05004 (2006).
4. U. A. Dyudina *et al.*, *Geophys. Res. Lett.* **37**, L09205 (2010).
5. A. Sanchez-Lavega, J. Lecacheux, F. Colas, J. F. Rojas, J. M. Gomez, *Planet. Space Sci.* **47**, 1277 (1999).
6. L. N. Fletcher *et al.*, *Icarus* **208**, 337 (2010).
7. A. Sanchez Lavega, *Icarus* **49**, 1 (1982).
8. A. Sanchez-Lavega *et al.*, *Nature* **353**, 397 (1991).
9. J. A. Westphal *et al.*, *Icarus* **100**, 485 (1992).
10. R. F. Beebe, C. Barnet, P. V. Sada, A. S. Murrell, *Icarus* **95**, 163 (1992).
11. C. D. Barnet, J. A. Westphal, R. F. Beebe, L. F. Huber, *Icarus* **100**, 499 (1992).
12. J. R. Acarreta, A. Sanchez-Lavega, *Icarus* **137**, 24 (1999).
13. Materials and methods are available as supporting material on *Science* Online.
14. P. L. Read *et al.*, *Planet. Space Sci.* **57**, 1682 (2009).
15. A. Sanchez-Lavega, J. F. Rojas, P. V. Sada, *Icarus* **147**, 405 (2000).
16. F. M. Flasar *et al.*, *Space Sci. Rev.* **115**, 169 (2004).
17. R. Hueso, A. Sanchez-Lavega, *Icarus* **172**, 255 (2004).
18. K. M. Sayanagi, A. P. Showman, *Icarus* **187**, 520 (2007).
19. S. Guerlet, T. Fouchet, B. Bézard, A. A. Simon-Miller, F. M. Flasar, *Icarus* **203**, 214 (2009).
20. P. Irwin *et al.*, *J. Quant. Spectrosc. Radiat. Transf.* **109**, 1136 (2008).
21. L. N. Fletcher, G. S. Orton, N. A. Teanby, P. G. J. Irwin, *Icarus* **202**, 543 (2009).
22. R. H. Brown *et al.*, *Space Sci. Rev.* **115**, 111 (2004).
23. P. O. Lagage *et al.*, *The Messenger* **117**, 12 (2004).

Acknowledgments: L.N.F. is supported by a Glasstone Science Fellowship at the University of Oxford. We thank members of both the Cassini CIRS and VIMS teams for their support in the analysis of Cassini data, and the director and staff of the ESO VLT for their assistance with the execution of these observations. This investigation was partially based on observations acquired at the Paranal UT3/Melipal Observatory under ID 386.C-0096. We are extremely grateful to all those observers contributing to the International Outer Planets Watch Planetary Visual Observatory & Laboratory (IOPW-PVOL), including T. Barry (Australia) for his contribution to Fig. 1. The UK authors acknowledge the support of the Science and Technology Facilities Council. A.S.L., R.H., and T.d.R. are supported by the Spanish MICIIN (Spanish Ministry of Science and Innovation) project AYA2009-10701 with FEDER and Grupos Gobierno Vasco IT-464-07. G.S.O. is supported by grants from NASA to the Jet Propulsion Laboratory, California Institute of Technology. L.N.F. performed the optimal estimation retrievals on both ground-based and space-based data sets and analyzed the results, and wrote the initial draft. B.E.H., G.L.B., and A.S.-M. designed the CIRS mapping observations; calibration assistance was provided by A.M. T.W.M. and K.H.B. provided the VIMS nightside spectra. G.S.O. supported ground-based VLT observations, and A.S.-L., R.H., and T.d.R.-G. provided IOPW-PVOL images. J.M.G. provided cylindrical mapping of IOPW-PVOL images. P.G.J.I. developed the optimal estimation retrieval codes used in this study. All authors discussed the results and commented on the manuscript.

Supporting Online Material

www.sciencemag.org/cgi/content/full/science.1204774/DC1
Materials and Methods
Figs. S1 to S5
Table S1
References (*24*–*28*)

24 February 2011; accepted 9 May 2011
Published online 19 May 2011;
10.1126/science.1204774

The 2010 M_w 8.8 Maule Megathrust Earthquake of Central Chile, Monitored by GPS

C. Vigny,[1]* A. Socquet,[2] S. Peyrat,[3] J.-C. Ruegg,[2] M. Métois,[1,2] R. Madariaga,[1] S. Morvan,[1] M. Lancieri,[1] R. Lacassin,[2] J. Campos,[3] D. Carrizo,[4] M. Bejar-Pizarro,[2] S. Barrientos,[3,5] R. Armijo,[2] C. Aranda,[5]† M.-C. Valderas-Bermejo,[5]† I. Ortega,[5]† F. Bondoux,[6]‡ S. Baize,[7]‡ H. Lyon-Caen,[1]‡ A. Pavez,[3]‡ J. P. Vilotte,[2]‡ M. Bevis,[8]§ B. Brooks,[9]§ R. Smalley,[10]§ H. Parra,[11]§ J.-C. Baez,[12]§ M. Blanco,[13]§ S. Cimbaro,[14]§ E. Kendrick[8]§

Large earthquakes produce crustal deformation that can be quantified by geodetic measurements, allowing for the determination of the slip distribution on the fault. We used data from Global Positioning System (GPS) networks in Central Chile to infer the static deformation and the kinematics of the 2010 moment magnitude (M_w) 8.8 Maule megathrust earthquake. From elastic modeling, we found a total rupture length of ~500 kilometers where slip (up to 15 meters) concentrated on two main asperities situated on both sides of the epicenter. We found that rupture reached shallow depths, probably extending up to the trench. Resolvable afterslip occurred in regions of low coseismic slip. The low-frequency hypocenter is relocated 40 kilometers southwest of initial estimates. Rupture propagated bilaterally at about 3.1 kilometers per second, with possible but not fully resolved velocity variations.

High-resolution geodetic data describing the static and dynamic rupture of a giant [moment magnitude (M_w) ≥ 8.5] earthquake have been recorded only a few times. Even in these few cases, monitoring deformation in the near field—at distances comparable to the size of the earthquake—is a major challenge. For example, it is still unclear why and how the rupture of the 2004 M_w 9.2 Sumatra earthquake extended beyond its original 400-km length, breaking through a plate boundary and becoming a giant earthquake at this instant (*1*, *2*). The M_w 8.8 Maule megathrust earthquake of 27 February 2010 occurred in the previously identified Concepción-Constitución seismic gap in central Chile. This gap had been defined from the size of the 1835 M_w 8.5 earthquake inferred from descriptions by Darwin and Fitzroy (*3*, *4*) (Fig. 1). Long-term

[1]Laboratoire de Géologie de l'Ecole Normale Supérieure, UMR CNRS 8538, Paris, France. [2]Institut de Physique du Globe de Paris et Université Paris-Diderot (Sorbonne Paris-Cité), UMR CNRS 7154, Paris, France. [3]Departamento de Geofisica, Universidad de Chile, Santiago, Chile. [4]Advanced Mining Technology Center, Universidad de Chile, Santiago, Chile. [5]Servicio Sismologico Nacional, Universidad de Chile, Santiago, Chile. [6]Institut pour la Recherche et le Développement, Lima, Peru. [7]Institut de Radioprotection et de Sûreté Nucléaire, Fontenay-aux-Roses, France. [8]School of Earth Sciences, Ohio State University, Columbus, OH 43210, USA. [9]Hawaii Institute of Geophysics and Planetology, University of Hawaii, Honolulu, HI 96822, USA. [10]Center for Earthquake Research and Information, University of Memphis, Memphis, TN 38152, USA. [11]Instituto Geográfico Militar, Santiago, Chile. [12]Universidad de Concepcion, Los Angeles, Chile. [13]Universidad Nacional de Cuyo, Argentina. [14]Instituto Geográfico Nacional, Argentina.

*To whom correspondence should be addressed. E-mail: vigny@biotite.ens.fr
†Servicio Sismologico Nacional team.
‡Laboratoire International Associé Montessus de Ballore postseismic team.
§Central and Southern Andes GPS Project team.

forecasts of large earthquakes in this zone were made using the seismic gap concept and historical seismicity (*5*–*8*); several mature gaps were identified with this method (*9*). Over the past decade, an array of geodetic markers were episodically resurveyed and more than 20 continuous Global Positioning System (cGPS) stations were deployed in the region between 37°S and 28°S. During the 10 years that preceded the 2010 event, the subduction interface in the Concepción-Constitución gap was fully coupled. If we extend this complete coupling to the past 175 years, a slip deficit of ~12 m had been accumulated because of plate convergence at ~7 cm/year (*10*), rendering the occurrence of

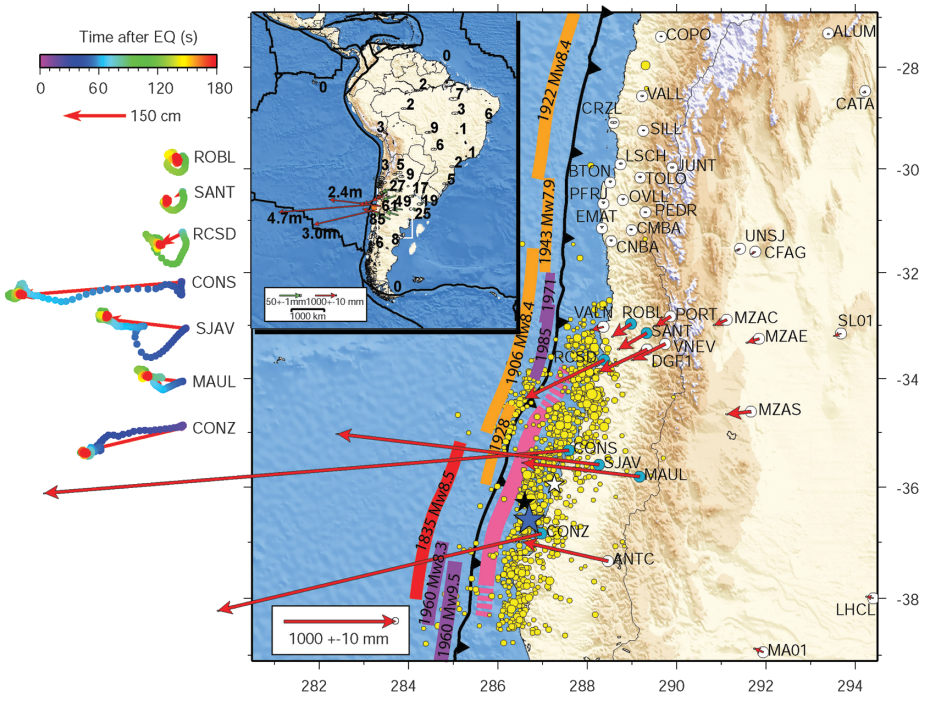

Fig. 1. Coseismic static displacement field derived from cGPS sites. Bold numbers next to arrowheads give the displacement in millimeters, except for the >1-m displacements in the continental scale inset (given in meters). Ellipses depict the 99% confidence level of formal uncertainties. Thin black lines depict plate boundaries. Stars depict hypocenter locations: NEIC (white), SSN (black), this study (red). Small yellow dots plot the locations of 1 month of aftershocks (NEIC). Color stripes along the trench depict past earthquake rupture zones (*6*–*12*). ETOPO-5 and GTOPO-30 Digital Elevation Models were used to generate the background topography and bathymetry. Color-coded curves next to displacement arrows at selected sites (left column) depict the path followed by these stations during the earthquake (1 position per second).

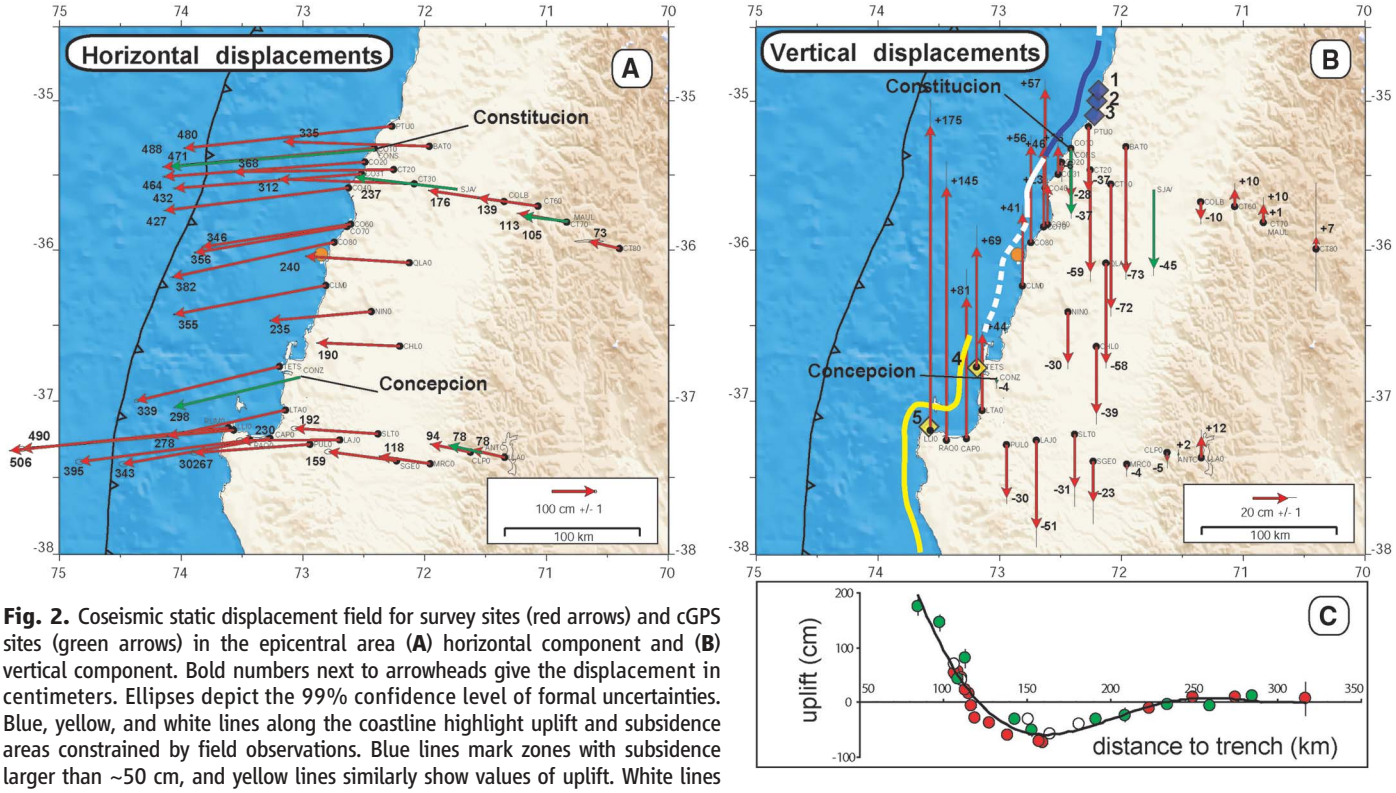

Fig. 2. Coseismic static displacement field for survey sites (red arrows) and cGPS sites (green arrows) in the epicentral area (**A**) horizontal component and (**B**) vertical component. Bold numbers next to arrowheads give the displacement in centimeters. Ellipses depict the 99% confidence level of formal uncertainties. Blue, yellow, and white lines along the coastline highlight uplift and subsidence areas constrained by field observations. Blue lines mark zones with subsidence larger than ~50 cm, and yellow lines similarly show values of uplift. White lines mark zones where vertical movement is difficult to evaluate because it is close to zero (± several tens of cm); dashed lines indicate where data are scarce or lacking. Sites discussed in SOM text are marked by numbered diamonds. The lower box (**C**) plots a cross section of land-level changes as a function of distance to the trench. Data are sorted by latitude: near Constitucion latitude (35.5°S to 36°S) (red circles), near Arauco-Concepcion latitude (37°S to 37.5°S) (green circles), and intermediate latitudes (white circles). The solid line shows the general trend, including all latitudes.

an earthquake of magnitude $M_w \geq 8$ possible (*11*–*13*).

We analyzed cGPS and survey GPS data from before, during, and after the Maule event to determine the deformation of Earth's surface close to the earthquake rupture (*14*). From these data, we identified the main asperities, quantified the spatial extent of the rupture, and determined whether rupture propagated up to the trench. We attempted to identify those features of the rupture propagation that explain why the Maule event became a megathrust earthquake.

Far-field cGPS stations more than 3000 km away from the epicenter, in Brazil, French Guyana, South Patagonia, and Galapagos, were unaffected by the earthquake. They provide a fixed reference frame together with several stations on the Brazilian craton that recorded displacements smaller than 1 cm (Fig. 1 and table S1). Closer to the hypocenter, in Argentina from 25°S to 45°S, the displacement field points in a concentric way toward the area of the epicenter and shows two distinct directions pointing to two main patches of deformation, south and north of the epicenter originally located at 36°S and 73°W. In Chile, this pattern becomes even more apparent, and campaign data confirm this trend (Fig. 2 and table S2). The maximum horizontal displacement of 5 m was observed both at the tip of the Arauco peninsula [Llico (LLI)/Rumena (RUM), ~80 km from the trench] and near Constitucion (CONS/CO1) [Laguna LlauLlau (CO2), Putu (PTU), ~120 km from the trench]. This is an indication that slip was larger in front of Constitucion than close to Concepcion (CONZ), contradicting some initial models that assigned little slip to this area (*14*). The relatively small displacement (70 cm) at San Antonio (RCSD) (33.5°S) indicates that even if some slip occurred there, the bulk of the rupture did not reach this latitude.

Vertical displacements reach 1.8 m of uplift at the tip of the Arauco peninsula, the land point closest to the trench (Fig. 2 and table S2). GPS markers along the coast show uplift, converting to subsidence 15 km south of Constitucion (+16 cm at CO3, –6 cm at CO2) and northward, where the coastline moves away from the trench. Along the coast, natural and anthropogenic markers also recorded the coseismic vertical displacements of the crust relative to sea level (Fig. 2). The pattern of subsidence and uplift deduced from such observations at five sites is compatible and complementary with GPS measurements if we take into account an uncertainty of several tens of cm (*14*). In the central valley, subsidence prevails (–30 to –70 cm), and small but resolvable uplift is observed in the Andes [+10 cm at Laguna de Laja (LLA) and Paso del Maule (CT8)]. Uplift and subsidence regions are roughly parallel to the trench (like the interseismic elastic pattern), regardless of the distribution of slip. Therefore, markers at different latitudes lay on the same cross section, revealing that the hinge line (the neutral line of vertical deformation of the upper plate) is located ~120 km from the trench (Fig. 2C).

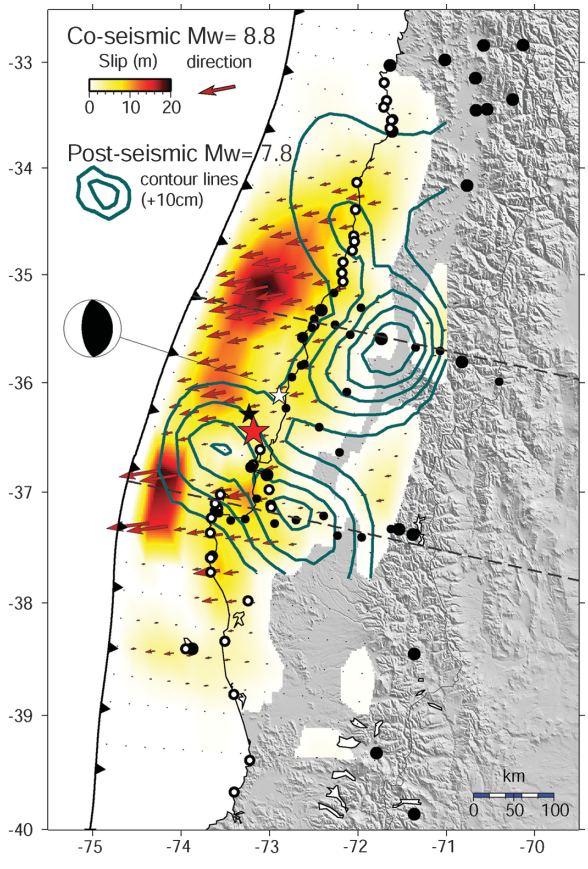

Fig. 3. Coseismic and afterslip source models. Red colors show the extent and the amount of coseismic slip (scale from 0 to 20 m). Dark red arrows depict the amount and direction of slip on the fault plane. Blue contour lines show the 12-day postseismic afterslip (contour level every 10 cm). Dots show locations and data type used in the inversion (black dots for GPS data: small for survey markers and large for cGPS stations; open dots for land-level data from natural or anthropogenic marker). Stars show hypocenter locations: NEIC (white), SSN (black), this study (red). The two dashed lines depict the profiles of fig. S1.

Postseismic deformation results from a combination of different phenomena, each of which has a characteristic time scale. Deformation occurring over a typical time scale of a month mostly represents immediate afterslip due to either aseismic slip in the poorly consolidated sedimentary layer overlying the fault, coseismic slip produced by the aftershock sequence, or silent slow-slip events that could have been triggered by changes in stress and friction produced by the main shock. Postseismic deformation started immediately after the earthquake (fig. S2 and table S3). Along the coastline, displacements of up to 15 cm were detected at CONZ over a 12-day period after the earthquake. There is less afterslip at CONS, with only 7 cm during the same period of time, although coseismic slip was larger there (5 m versus 3 m). On the other hand, afterslip is as large at RCSD (6 cm), although almost no coseismic slip occurred there. This may be an indication of a triggered slow-slip event at this latitude and may explain the large number of aftershocks generated in this area. In addition, the direction of postseismic deformations (almost westward) is not parallel to coseismic displacements. Thus, postseismic slip may be occurring on different patches and/or with a different direction than the coseismic slip. Finally, postseismic deformation inland is large: Colbun (MAUL) (200 km inland) moved even more than CONS, with 10 cm of displacement. This is an indication of the depth and long reach of the postseismic process that affects the region below the seismogenic zone.

To better constrain the earthquake slip distribution, we combined our data with published land-level changes, several additional GPS displacements, and Wide Swath Alos fringes provided by the Japanese Aerospace Exploration Agency (JAXA) and the National Research Institute for Earth Science and Disaster Prevention (NIED) (*15*, *16*). The surface deformation fields associated with the coseismic and postseismic phases were modeled using Okada's formulation of the elastic field due to a rectangular dislocation buried in an elastic half-space (*14*). The earthquake broke a ~500-km-long portion of the subduction interface (~450 km with slip larger than 2 m), extending along strike from 38.2°S to 34°S and from 5-km to 45-km depth (Fig. 3). The area that ruptured corresponds very closely with the highly coupled zone detected by interseismic GPS measurements (*13*, *17*). With a shear modulus of 3.3 10^{10} Pa, our slip distribution yields an equivalent geodetic moment of 1.76 10^{22} N·m (M_w 8.76), in agreement with seismological estimates (M_w = 8.8). The coseismic slip is distributed into two main patches of slip, reaching a maximum of 15 m. The patches are separated by a zone of reduced slip (<4 m) near latitude 36.5°S; this is the same area where we relocated the epicenter using the high-rate cGPS data. The northern patch of slip accounts for 62% of the geodetic moment (1.09 10^{22} N·m, M_w 8.62), and the southern patch of slip accounts for the other 38%.

Our dense near-field data, in particular the large values of horizontal versus vertical displacement along the coast, require that ~60% of the slip (equivalent to an M_w 8.6 event) occur at shallow depths (<25 km and close to the trench). Such shallow slip was detected by earlier models based on seismological data (*18*) but was not found in models using far-field data only and/or interferometric synthetic aperture radar (*16*, *19*, *20*). The comparison of the surface displacements predicted by published models against our data shows that they systematically underestimate the static horizontal displacements (*14*). The shallower part of the subduction zone is usually considered as an area of stable sliding characterized by rate-strengthening behavior (*21*). Thus, the fact that the rupture broke all the way up to the sea-bottom at the trench may be surprising. However, shallow slip is consistent with the generation of a powerful tsunami and the presence of numerous aftershocks located near the trench (Fig. 1). At greater depths, slip decreases smoothly and vanishes at about 45-km depth everywhere along the coast; this is consistent with the hinge line localization 120 km away from the trench (Fig. 2C). With a dip angle of 17° to 20°, the down-dip end of the rupture is located at the bottom of the seismogenic zone.

Postseismic motions during the 12 days after the earthquake can be modeled as afterslip on the subduction interface, accounting for 4% of the coseismic moment. Several centimeters (5 to 10) of westward motion may have occurred on some near-field coastal stations during the half day after the earthquake (fig. S3). This is also consistent with a logarithmic decrease with time of postseismic displacements shown by our 12-day time series (fig. S2). However, these displacements are too small to support the occurrence of an intense rapid afterslip up to 20% of the coseismic slip suggested from normal modes excitation (*22*).

Our near-field data are sparse, so some variability in the models exists. We observe the following features: (i) deep slip (30 to 60 cm) between 40-km and 65-km depth that accounts for 56% of the 12-day afterslip; (ii) 10 to 20 cm of slip (23% of the 12-day afterslip) near the northern edge of the rupture, close to Pichilemu (34.5°S), where a large aftershock occurred on 11 March 2010 on a shallow normal fault; (ii) 30 to 40 cm of localized slip (21% of the 12-day afterslip) occurring at seismogenic depths, near 36.5°S, close to the epicenter where coseismic slip had a minimum between the two main asperities. Coseismic and postseismic distributions of slip complement each other (Fig. 3), suggesting an interlacing of "velocity strengthening" areas (prone to stable slip) and "velocity weakening" areas (where stick-slip occurs). The equivalent magnitude of our postseismic model (M_w 7.8) is larger than the cumulated moment of the aftershocks (~M_w 7) in the same 12-day period after the main shock, implying that most (~90%) of the postseismic deformation was released by aseismic slip on the subduction interface. Additionally, 56% of the afterslip occurred below 35-km depth. Considering that viscous relaxation in the mantle cannot occur in this short time scale of only a few days, we conclude that aseismic slip occurred on the deep subduction interface.

In addition to a 24-hour average position, it is also possible to compute each station position at the sampling rate of the GPS signal (1 s at most stations) (*14*). We refer to these GPS records as "motograms," which are actually low-frequency seismograms with two important differences: (i) they directly measure ground displacement, eliminating the unstable double integration of accelerograms; (ii) they do not saturate, whatever the amplitude of the ground displacement. In the case of a megathrust earthquake, aliasing due to the low sampling rate of cGPS (1 Hz) is not a problem (*14*). *S* waves on near-field motograms could be clearly identified, as is demonstrated by the comparison with collocated accelerograms at station El Roble in central Chile (see ROBL in fig. S4). *P* waves were more difficult to read because stations in central Chile lie close to a nodal plane of the earthquake. The need for relocation of the epicenter is obvious from the motograms recorded at CONS and CONZ (Fig. 4). *S* waves arrive at CONZ about 20 s before they arrive at CONS. Using *S* waves measured in the motograms [mainly CONZ, CONS, San Javier (SJAV), MAUL, RCSD, and ROBL], we determined a low-frequency epicentral location at 36.41°S and 73.18°W. This epicenter is different from those reported by seismological services. It is located 15 km south of the epicenter by the Servicio Sismologico Nacional (SSN) of the University of Chile that located it at 36.29°S, 73.24°W and is almost 40 km southwest of the epicenter reported by the National Earthquake Information Center (NEIC) in its weekly Earthquake Data Report (36.12°S, 72.89°W).

With a relocated epicenter, we found that the displacement at the four GPS stations in the near field is dominated by the static field (final static offsets are 10 times as large as dynamic displacements) (Fig. 4). All the near-field stations (CONS to RCSD) resemble the displacement expected near a large crack propagating at high subshear speed (Figs. 1 and 4). We tested several source models with rupture starting from the epicenter and propagating at constant speed. Stations located in the north, RCSD and ROBL, are the most sensitive to rupture speed because of directivity. As expected from dynamic fault modeling, CONS and CONZ, located practically on top of the fault, are dominated by slip near the stations. We found that rupture speeds between 2.8 and 3.1 km/s produce good fit between synthetics and observed motograms (Fig. 4). The displacement functions observed at CONS and CONZ are very

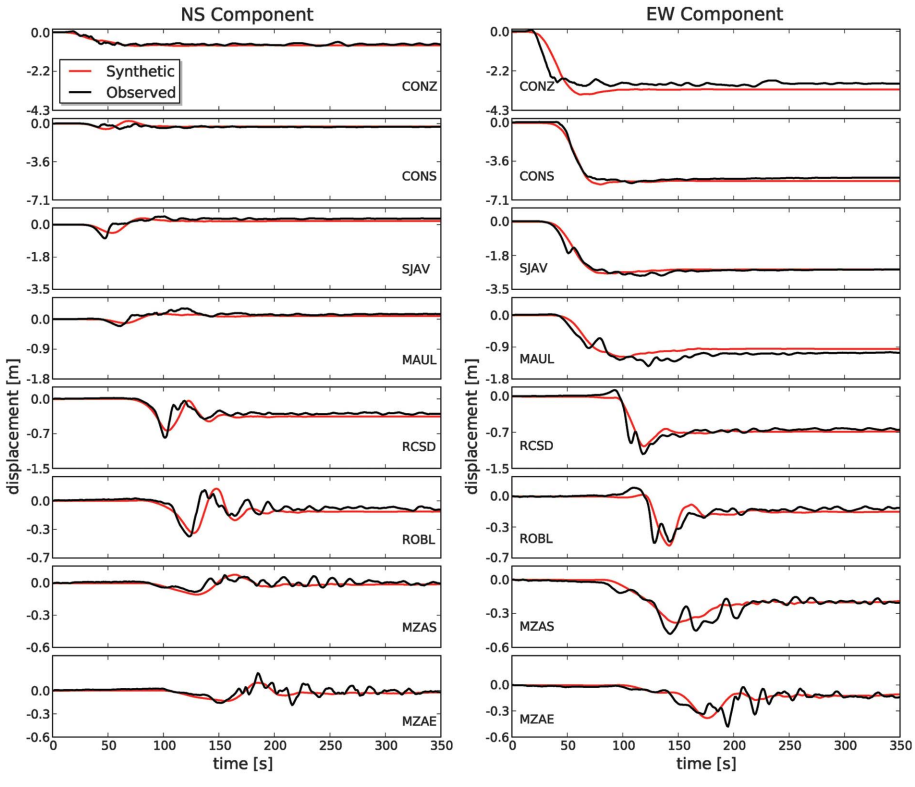

Fig. 4. Observed motograms at eight cGPS stations in central Chile and Western Argentina (red lines) compared with synthetics (black lines) computed using the slip distribution shown in Fig. 3. Displacement scale is in meters; elapsed time is in seconds. In this model, rupture starts from the low-frequency epicenter located at 36.41°S, 73.18°W, determined from the *S* wave arrivals at motograms and accelerograms in central Chile. Rupture propagated radially away from the epicenter at a speed of 3.1 km/s, and the rise time was uniform on the fault and equal to 20 s.

similar to those of a simple shear fault propagating along the seismogenic zone. The rise time at both stations is close to 20 s, so that we can approximate the width of the fault as twice (because of upward and downward propagation) the product of this time multiplied by the rupture speed. We obtain a fault width of ~120 km, which is in agreement with our static modeling. Some motograms (especially SJAV) also reveal an arrival (or "kink") that may be due to a possible rupture velocity variation as rupture reaches the northern asperity (fig. S4). We attribute this arrival to the triggering of rupture in the northern asperity (the largest one), ~60 s after the initiation of the rupture. This arrival would mark the instant when the Maule event became a megathrust earthquake.

Comparing the 2010 Maule megathrust earthquake rupture with earlier events is important for seismic hazard assessment, but the lack of precise information about some past events requires caution. The 2010 rupture broke well beyond the previously identified gap left by the 1835 earthquake, which appears to have had a shorter rupture length of about 350 km and a smaller magnitude. The shorter rupture of 1835 corresponds roughly to the length attained by the 2010 rupture at the critical instant captured at 60 s in the motograms. This is before rupture of the main northern asperity, which may have reached the trench, thus contributing strongly to generation of the tsunami that struck the coast of Constitución (~5 m of minimum inundation over a large latitudinal extent). The absence of large tsunami at Constitución in 1835 (*4*) is consistent with lack of rupture of the northern asperity during that event. The 2010 rupture covered the M_w 7.6 Talca earthquake of 1928, which may have been an event located near the transition zone similar to the 2007 M_w 7.7 Tocopilla earthquake (*7*, *23*) in Northern Chile. The ~500-km-long 2010 rupture overlaps laterally (over ~100 km) also with the ruptures of three earthquakes that occurred earlier on its southern and northern edges: to the south, the 21 May 1960 Concepcion event (M_w 8.3) and the Valdivia earthquake of 22 May 1960 (M_w 9.5); to the north, the rupture zone of the 1906 M_w 8.5 Valparaíso earthquake. This suggests interleaved tapering of coseismic slip in those overlapping regions, probably involving, over the long term, accommodation of deformation by both seismic and aseismic processes.

References and Notes

1. R. Bilham, *Science* **308**, 1126 (2005).
2. C. Vigny *et al.*, *Nature* **436**, 201 (2005).
3. C. Darwin, *Journal of Researches into the Natural History and Geology of the Countries Visited During the Voyage of the H.M.S. Beagle Round the World* (John Murray, London, 1876).
4. R. FitzRoy, *Narrative of the Surveying Voyages of His Majesty's Ships Adventure and Beagle Between the years 1826 and 1836, Describing Their Examination of the Southern Shores of South America, and the Beagle's Circumnavigation of the Globe* (Henry Colburn, London, 1839).
5. F. Montessus de Ballore, *Historia Sismica de los Andes Meridionales, 6 vols.* (Editorial Cervantes, Santiago de Chile, 1916).
6. C. Lomnitz, *Geofis. Panamericana* **1**, 151 (1971).
7. S. L. Beck, S. Barrientos, E. Kausel, M. Reyes, *J. S. Am. Earth Sci.* **11**, 115 (1998).
8. R. Madariaga, M. Métois, C. Vigny, J. Campos, *Science* **328**, 181 (2010).
9. S. Nishenko, *J. Geophys. Res.* **90**, 3589 (1985).
10. Z. Altamimi, X. Collilieux, J. Legrand, B. Garayt, C. Boucher, *J. Geophys. Res.* **112**, B09401 (2007).
11. J. Campos *et al.*, *Phys. Earth Planet. Inter.* **132**, 177 (2002).
12. J. C. Ruegg *et al.*, *Geophys. Res. Lett.* **29**, 1517 (2002).
13. J. C. Ruegg *et al.*, *Phys. Earth Planet. Inter.* **175**, 78 (2009).
14. Materials and methods are available as supporting material on *Science* Online.
15. M. Farías *et al.*, *Science* **329**, 916 (2010).
16. X. Tong *et al.*, *Geophys. Res. Lett.* **37**, L24311 (2010).
17. M. Moreno, M. Rosenau, O. Oncken, *Nature* **467**, 198 (2010).
18. T. Lay *et al.*, *Geophys. Res. Lett.* **37**, L13301 (2010).
19. B. Delouis, J.-M. Nocquet, M. Vallée, *Geophys. Res. Lett.* **37**, L17305 (2010).
20. S. Lorito *et al.*, *Nat. Geosci.* **4**, 173 (2011).
21. R. D. Hyndman, M. Yamano, D. A. Oleskevich, *Isl. Arc* **6**, 244 (1997).
22. T. Tanimoto, C. Ji, *Geophys. Res. Lett.* **37**, L22312 (2010).
23. M. Béjar-Pizarro, D. Carrizo, A. Socquet, R. Armijo, and the North Chile Geodetic Team, *Geophys. J. Int.* (2010).

Acknowledgments: We thank the International GNSS Service; Instituto Geográfico Nacional, Argentina; Instituto Brasileiro de Geografia e Estatística, Brasil; and Transportable Integrated Geodetic Observatory/ Bundesamt für Kartographie und Geodäsie Frankfurt/ Universidad de Concepcion for access to their cGPS data in South America. We are also thankful to the French Institut National des Sciences de l'Univers, the Institut pour la Recherche et le Développment, the Agence Nationale pour la Recherche, and the Ministère des Affaires Etrangères for providing financial support. We also thank members of the Laboratoire International Associé Montessus de Ballore and the many individuals who participated in field campaigns and network maintenance over the years. This is IPGP contribution #3161.

Supporting Online Material

www.sciencemag.org/cgi/content/full/science.1204132/DC1
Materials and Methods
SOM Text
Figs. S1 to S14
Tables S1 to S4
References (*24*–*35*)

10 February 2011; accepted 20 April 2011
Published online 28 April 2011;
10.1126/science.1204132

The 2011 Magnitude 9.0 Tohoku-Oki Earthquake: Mosaicking the Megathrust from Seconds to Centuries

Mark Simons,[1]* Sarah E. Minson,[1] Anthony Sladen,[1,2] Francisco Ortega,[1] Junle Jiang,[1] Susan E. Owen,[3] Lingsen Meng,[1] Jean-Paul Ampuero,[1] Shengji Wei,[1] Risheng Chu,[1] Donald V. Helmberger,[1] Hiroo Kanamori,[1] Eric Hetland,[4] Angelyn W. Moore,[3] Frank H. Webb[3]

Geophysical observations from the 2011 moment magnitude (M_w) 9.0 Tohoku-Oki, Japan earthquake allow exploration of a rare large event along a subduction megathrust. Models for this event indicate that the distribution of coseismic fault slip exceeded 50 meters in places. Sources of high-frequency seismic waves delineate the edges of the deepest portions of coseismic slip and do not simply correlate with the locations of peak slip. Relative to the M_w 8.8 2010 Maule, Chile earthquake, the Tohoku-Oki earthquake was deficient in high-frequency seismic radiation—a difference that we attribute to its relatively shallow depth. Estimates of total fault slip and surface secular strain accumulation on millennial time scales suggest the need to consider the potential for a future large earthquake just south of this event.

The 2011 Tohoku-Oki earthquake occurred on the megathrust where the Pacific Plate subducts below Japan at an average rate of about 8 to 8.5 cm/year (Fig. 1) (*1*). Historically, many moment magnitude (M_w) 7 to M_w 8 earthquakes have occurred on the Japan Trench megathrust (*2*). Geodetic observations of crustal strain during the interseismic period have been used to infer spatial variations in the degree of plate coupling (i.e., regions of the megathrust expected to produce large earthquakes) for this section of the Japan Trench (*3*). Generally, these models infer high coupling in regions where earthquakes were known to have already occurred (Fig. 1 and fig. S1), with only partial or even no coupling from the trench to a point approximately midway between the trench and the coastline—precisely the region where the 2011 Tohoku-Oki earthquake occurred. It is fundamentally difficult to use land-based data to assess the state of coupling on distant portions of a megathrust. The Jogan earthquake of 13 July 869 may be the only documented event to have occurred with a possible magnitude and location similar to that of the 2011 earthquake (*4*).

Observations of the 2011 Tohoku-Oki earthquake from a dense regional geodetic network

[1]Seismological Laboratory, Division of Geological and Planetary Sciences, California Institute of Technology, Pasadena, CA 91125, USA. [2]Geoazur, Observatoire de la Côte d'Azur, Université de Nice–Sophia Antipolis, CNRS, IRD, Valbonne, 06103 Nice Cedex 2, France. [3]Jet Propulsion Laboratory, California Institute of Technology, Pasadena, CA 91109, USA. [4]Department of Geological Sciences, University of Michigan, Ann Arbor, MI 48109, USA.

*To whom correspondence should be addressed. E-mail: simons@caltech.edu